Science
AAAS

Protein Friction Limits Diffusive and Directed Movements of Kinesin Motors on Microtubules

Volker Bormuth, *et al.*

Science **325**, 870 (2009);
DOI: 10.1126/science.1174923

These changes in sleep homeostasis in the mutant mice provide a testable hypothesis for future work examining why human subjects with the mutation lead such active lives despite their persistently shorter sleep.

We performed EEG and EMG on *Dec2* KO mice and their WT littermates. Baseline wakefulness, NREM, and REM percentages showed that *Dec2* KO mice sleep slightly more than the WT mice and that the difference is mostly in the dark period (table S4 and fig. S2). During the light period, only the NREM sleep of *Dec2* KO mice was more abundant than that of WT mice and only slightly so. NREM rebound after sleep deprivation for *Dec2* KO mice was much slower, which implied that Dec2 is an important factor regulating sleep recovery.

We next set out to test whether m*Dec2P385R* can cause a similar rest-sleep phenotype in *Drosophila*. The closest homologous protein to DEC2 in *Drosophila* [CG17100, clockwork orange (*16*, *17*)] shares <18% amino acid sequence similarity, <11% identity, and P385 is not conserved. We therefore generated transgenic flies with expression-inducible UAS-*mDec2WT* and UAS-*mDec2P385R* on the *w1118* background. When these flies were crossed with *elav*-GAL4, driving pan-neuronal overexpression (*18*), *mDec2P385R* flies showed significantly lower daytime sleep-like behavior with reduced rest bout number and lengthened rest bout durations compared with WT flies (Fig. 4A). Because mushroom bodies were shown to be the likely sleep-rest behavior center in *Drosophila* (*19*), we also overexpressed P385R and WT m*Dec2* under the control of a mushroom body *30Y*-GAL4 driver (*20*). It was noteworthy that *mDec2P385R* transgenic flies driven by the *30Y*-GAL4 showed significantly less sleeplike behavior with significantly shorter sleep bout duration in both light and dark phases than *mDec2WT* flies (Fig. 4B). However, rest or sleep bout number was significantly higher only in the dark phase for *mDec2P385R* transgenic flies. These results indicate that the behavior of flies with mushroom body driver expression of *mDec2P385R* echoed those of the *DEC2-P385R* transgenic mice (Fig. 2, B, C, and E, and Fig. 4B).

The power of human genetics in studying human behavioral traits was demonstrated in the identification of mutations and the subsequent molecular characterization of FASPS (*21*–*23*). As currently understood, FASPS is primarily a circadian rhythm variant leading to altered phase; total daily sleep time is normal (*21*, *23*, *24*). We have applied a similar approach and identified a gene involved in regulation of sleep quantity. This provides a unique opportunity for exploring human sleep quantity regulation. *DEC2-P385R* mutation gave a short sleep phenotype, which was recapitulated in transgenic mouse and fly models but was not found in *Dec2* KO mice. In addition, this phenotype was enhanced by the absence of endogenous *Dec2* alleles, which suggested that P385R leads to a dominant-negative mutation. Our results demonstrate that *DEC2* plays an important role in regulating daily total sleep time in mammals and that the control of sleep-like behavior may be conserved and regulated in a similar manner as far back in evolution as invertebrates.

We did not see statistically significant differences in the NREM delta or REM theta power in the *DEC2-P385R* mice during day- or night-time sleep, although there is a trend toward increased NREM delta in these mice. It is possible that a small deficit of sleep in the short term does not significantly affect sleep power, whereas a long-term accumulation will. Alternatively, the attenuated NREM delta power enhancement, together with slow and incomplete NREM sleep recovery after sleep deprivation in the *DEC2-P385R* mice, suggests that these mice are able to cope with shorter sleep because of altered sleep homeostasis. It is noteworthy that recent data on human sleep emphasizes the importance of cumulative sleep debt even if it is only due to partial sleep deprivation. Understanding the regulatory mechanisms of sleep quality and quantity will facilitate the development of interventions to alleviate pathologies associated with sleep disturbance.

References and Notes

1. P. M. Fuller, J. J. Gooley, C. B. Saper, *J. Biol. Rhythms* **21**, 482 (2006).
2. C. B. Saper, T. C. Chou, T. E. Scammell, *Trends Neurosci.* **24**, 726 (2001).
3. E. F. Pace-Schott, J. A. Hobson, *Nat. Rev. Neurosci.* **3**, 591 (2002).
4. J. S. Durmer, D. F. Dinges, *Semin. Neurol.* **25**, 117 (2005).
5. K. L. Knutson, E. Van Cauter, *Ann. N. Y. Acad. Sci.* **1129**, 287 (2008).
6. H. P. Van Dongen, G. Maislin, J. M. Mullington, D. F. Dinges, *Sleep* **26**, 117 (2003).
7. H. S. Akiskal, K. K. Akiskal, R. F. Haykal, J. S. Manning, P. D. Connor, *J. Affect. Disord.* **85**, 3 (2005).
8. H. Hamaguchi *et al.*, *Biochem. J.* **382**, 43 (2004).
9. S. Honma *et al.*, *Nature* **419**, 841 (2002).
10. M. J. Rossner *et al.*, *PLoS One* **3**, e2762 (2008).
11. M. E. Massari, C. Murre, *Mol. Cell. Biol.* **20**, 429 (2000).
12. Materials and methods are available as supporting material on *Science* Online.
13. J. Kondo *et al.*, *Int. J. Mol. Med.* **17**, 1053 (2006).
14. M. Noshiro *et al.*, *J. Biol. Rhythms* **20**, 404 (2005).
15. P. Franken *et al.*, *Proc. Natl. Acad. Sci. U.S.A.* **103**, 7118 (2006).
16. S. Kadener, D. Stoleru, M. McDonald, P. Nawathean, M. Rosbash, *Genes Dev.* **21**, 1675 (2007).
17. C. Lim *et al.*, *Curr. Biol.* **17**, 1082 (2007).
18. Y. Q. Zhang, C. K. Rodesch, K. Broadie, *Genesis* **34**, 142 (2002).
19. W. J. Joiner, A. Crocker, B. H. White, A. Sehgal, *Nature* **441**, 757 (2006).
20. M. Y. Yang, J. D. Armstrong, I. Vilinsky, N. J. Strausfeld, K. Kaiser, *Neuron* **15**, 45 (1995).
21. C. R. Jones *et al.*, *Nat. Med.* **5**, 1062 (1999).
22. K. L. Toh *et al.*, *Science* **291**, 1040 (2001).
23. Y. Xu *et al.*, *Nature* **434**, 640 (2005).
24. Y. Xu *et al.*, *Cell* **128**, 59 (2007).

25. We thank A. Sehgal for elav-GAL4 *Drosophila* driver constructs; the Ishikawa laboratory in Kyoto University for pcDNA3-hSIRT1-FLAG constructs, H.-Y. Lee for technical support and L. J. Ptáček for insightful discussions and careful editing of the manuscript. This work was supported by NIH grant HL059596, Conte Center grant (MH074924), and by the Sandler Neurogenetics fund.

Supporting Online Material

www.sciencemag.org/cgi/content/full/325/5942/866/DC1
Materials and Methods
Figs. S1 and S2
Tables S1 to S4
References

22 May 2009; accepted 29 June 2009
10.1126/science.1174443

Protein Friction Limits Diffusive and Directed Movements of Kinesin Motors on Microtubules

Volker Bormuth,[1] Vladimir Varga,[1] Jonathon Howard,[1]* Erik Schäffer[2]*

Friction limits the operation of macroscopic engines and is critical to the performance of micromechanical devices. We report measurements of friction in a biological nanomachine. Using optical tweezers, we characterized the frictional drag force of individual kinesin-8 motor proteins interacting with their microtubule tracks. At low speeds and with no energy source, the frictional drag was related to the diffusion coefficient by the Einstein relation. At higher speeds, the frictional drag force increased nonlinearly, consistent with the motor jumping 8 nanometers between adjacent tubulin dimers along the microtubule, and was asymmetric, reflecting the structural polarity of the microtubule. We argue that these frictional forces arise from breaking bonds between the motor domains and the microtubule, and they limit the speed and efficiency of kinesin.

Friction is the force that resists the relative motion of two bodies in contact. Contact is mediated by adhesive bonds between individual molecules, and friction arises from the forces necessary to deform and break these bonds (*1*). When a bond breaks, the energy stored in its deformation is dissipated. Adhesive interactions occur between proteins (*2*, *3*), and how they might give rise to protein friction has been discussed theoretically (*4*). Protein friction is expected to be

especially important for motor proteins because these nanomachines bind stereospecifically to discrete sites on a filamentous track and because, in order to move, they must break the bond at one site before rebinding at a new site in the direction of motion. In theoretical models of force generation by molecular motors, protein friction is predicted to limit both speed and efficiency (*5*–*9*). However, the frictional forces acting on motors have not been measured, and how they depend on the speed and direction of motion is not known.

Protein friction is related to diffusion according to the Einstein relation, $D = k_B T/\gamma$ (D diffusion coefficient, k_B Boltzmann constant, T absolute temperature, γ frictional drag coefficient). The higher the protein friction, the slower the diffusion. Diffusion of proteins along polymers—i.e., randomly directed stepping, as opposed to the directed adenosine triphosphate (ATP)–driven stepping of motor proteins—is functionally important. In the case of microtubules, diffusion along the microtubule lattice rapidly targets proteins to the microtubule ends [MCAK and XMAP215 (*10*, *11*)]; maintains dynamic contact between chromosomes and the growing or shrinking ends of microtubules [Dam1 and Ndc80 (*12*, *13*)]; and allows sliding of bundled microtubules [Ase1p and Ncd (*14*, *15*)]. The diffusion coefficients vary by over three orders of magnitude, which implies that the frictional interactions must also vary considerably in strength. It has been hypothesized that the diffusive interaction between these proteins and microtubules is mediated by electrostatic forces between the negatively charged, glutamic acid–rich C termini of α and β tubulins (the E-hooks) and positively charged amino acids in the diffusing proteins (*16*). Because the E-hooks are spaced every 4 nm, this electrostatic model predicts 4-nm diffusive steps, different from the 8-nm directed steps between adjacent tubulin dimers that motor proteins such as kinesin take. However, the binding sites associated with diffusion, the size of the diffusive steps, and the relation between diffusion and protein friction has not been experimentally studied.

The interaction of budding yeast kinesin-8, Kip3p, with microtubules is an ideal model system in which to study protein friction and its relation to diffusion. Kinesin-8 motors accelerate depolymerization of microtubules (*17*, *18*) and thereby regulate the lengths of mitotic spindles in yeast and other cells (*19*). In the presence of ATP, Kip3p is a highly processive motor that moves toward the plus, or rapidly growing, end of the microtubule (*17*); however, in the absence of ATP, we found that it diffuses on the microtubule lattice for several seconds (Fig. 1, A and B). Using total internal reflection fluorescence (TIRF) microscopy (*20*), we measured the diffusion coefficient in adenosine diphosphate (ADP, 1 mM) from the mean-squared displacement to be D_{TIRF} = 0.0043 ± 0.0005 μm^2/s (Fig. 1C). (All errors are SEM unless otherwise noted.) The diffusion coefficient in the absence of nucleotides was much smaller, 0.00020 ± 0.00003 μm^2/s (fig. S1). The value of the diffusion coefficient in ADP corresponds to a frictional drag coefficient of γ_{TIRF} = 0.95 ± 0.11 μNs/m. This implies that imposed velocities on the order of $\upsilon \approx 1$ μm/s will lead to frictional forces of $\gamma\upsilon \approx 1$ pN, which should be measurable with optical tweezers.

We used optical tweezers (*21*, *22*) to directly measure the friction force between Kip3p and microtubules in the presence of ADP (*20*). To quantify the motor-filament interaction forces as a function of velocity, we dragged Kip3p-coated microspheres over immobilized microtubules (Fig. 2A). The concentration of Kip3p molecules on the microspheres was low enough to ensure that only single molecules interacted with the microtubule (*20*). We moved the microtubules relative to the laser trap back and forth with a constant speed, using a piezo-electric translation stage, and recorded the position of the Kip3p-coated microsphere. To correlate the friction forces with the polarity of the microtubule, we exchanged the buffer at the end of each experiment with one containing ATP and, for the same microtubule, identified the polarity by the plus end–directed motility of the Kip3p-coated microspheres.

A representative experiment in 1 mM ADP is shown (Fig. 2B) in which both the centroid of a microsphere and the center of the laser trap are plotted against time. Upon Kip3p binding (arrows), the microsphere transiently slowed down and then accelerated to follow the trap, lagging on average a constant displacement Δx behind the trap center. Using the calibrated trap stiffness κ_{trap} [~0.037 pN/nm (*21*, *23*)], we then calculated the friction force $F = \kappa_{trap}\Delta x$ during such drag events (Fig. 2C). After the transient response, the friction force reached a steady state (Fig. 2C, dashed lines) and its magnitude increased with increasing speed.

The motor-microtubule friction force depended on speed and, in the case of large speeds, additionally on direction (Fig. 3). For small stage speeds, υ, the friction force increased linearly according to $F = \gamma\upsilon$. In the experiment shown in Fig. 3, the frictional drag coefficient was 1.11 ± 0.07 μNs/m, in good agreement with γ_{TIRF} (no significant difference by a t test, t = 1.23, $P < 0.95$). This frictional drag coefficient was much larger than the hydrodynamic (viscous) drag coefficient of the molecule (fig. S3A) and microsphere (fig. S4). The frictional drag coefficients inferred from the initial slopes of nine force-velocity curves in 1 mM and 2 mM ADP (table S1) were in good agreement with the ones calculated from measurements of the diffusion coefficient at the same ADP concentrations (*20*). This agreement with the Einstein relation was expected because, in the presence of ADP, which does not serve as an energy source for kinesin motors, the system is close to thermal equilibrium. Thus, both the drag and the diffusion arise from bond rupture dynamics.

At higher velocities, the frictional forces depended nonlinearly on speed, leveled off, and were significantly lower when the motor was dragged toward the microtubule's plus end compared with the minus end (Fig. 3). The nonlinearity can be well accounted for by a model for protein friction in which an energy barrier has to be overcome to break an adhesive bond (*4*). The external force F_{trap} alters the diffusive stepping rate according to the Arrhenius theory (*9*). If there is a single energy barrier between adjacent binding sites, then the mean motor velocity υ_m is equal to the product of the step distance, δ, and the difference between the mean forward, k_+, and backward, k_-, stepping rates, which depend exponentially on the force:

$$\upsilon_m = \delta(k_+ - k_-) \text{with } k_\pm = k_0 e^{\pm F_{trap}(\frac{1}{2}\delta \pm \Delta)/(k_B T)} \quad (1)$$

where k_0 is the stepping rate without a force. The asymmetry parameter Δ corresponds to the distance between the midpoint of the binding

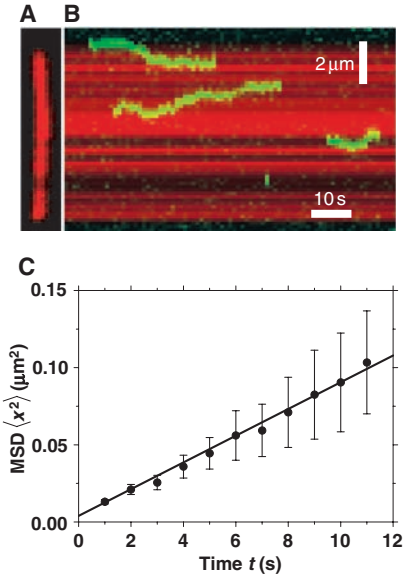

Fig. 1. Diffusion of Kip3p (kinesin-8) along microtubules in the presence of 1 mM ADP. (**A**) Image of a dimly rhodamine-labeled microtubule (red). (**B**) Kymograph of sequential frames of single Kip3p-GFP (green fluorescent protein) molecules (green) overlaid on the image of the microtubule (red) depicted in (A). (**C**) Mean-squared displacement MSD $\langle x^2 \rangle$ plotted against time t. A linear fit yielded the diffusion coefficient quoted in the text via $\langle x^2 \rangle = 2Dt + 2\varepsilon^2$ with tracking precision ε = 44 nm.

[1]Max Planck Institute of Molecular Cell Biology and Genetics, Pfotenhauerstrasse 108, 01307 Dresden, Germany. [2]Nanomechanics Group, Biotechnology Center, TU Dresden, Tatzberg 47-51, 01307 Dresden, Germany.

*To whom correspondence should be addressed. E-mail: Howard@mpi-cbg.de (J.H.); Erik.Schaeffer@biotec.tu-dresden.de (E.S.)

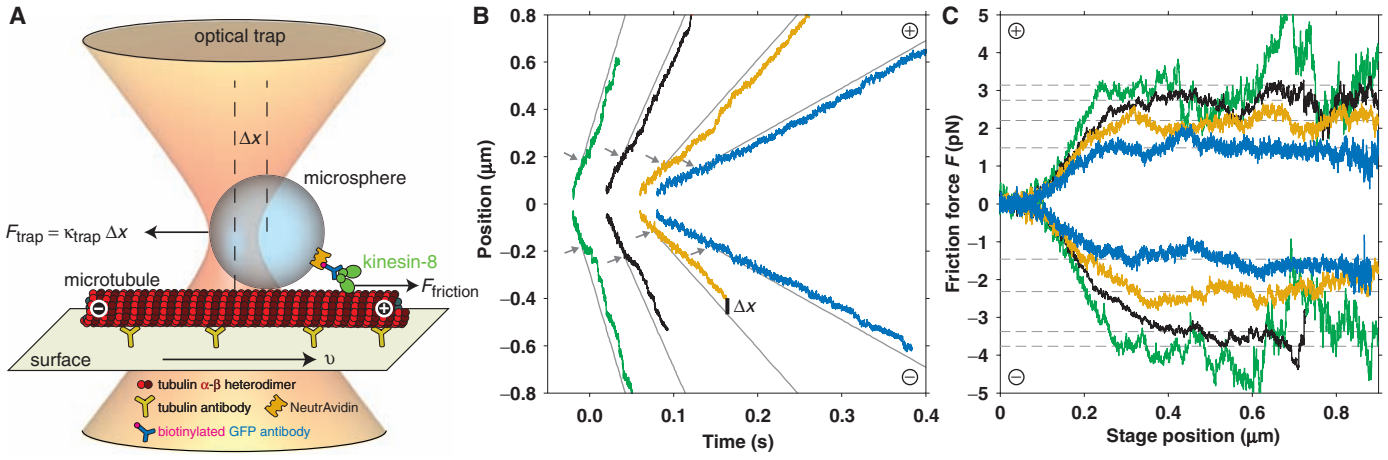

Fig. 2. Kip3p dragged over a microtubule in the presence of 1 mM ADP. (**A**) Schematic of the experiment: Using a focused laser, a Kip3p-coated microsphere is trapped close to an immobilized microtubule (not drawn to scale). Moving the stage with constant velocity υ past the stationary laser drags the microtubule lattice underneath the kinesin-8 molecule, creating a friction force $F = -F_{trap}$ (neglecting the very small hydrodynamic drag arising from the viscosity of the aqueous solution). Positive stage velocity is defined as the microtubule moving with its plus end leading; in this case, the laser and the motor are moving toward the minus end. (**B**) Time traces of the positions of the trap center (gray lines) and the microsphere relative to the microtubule plus end ($|\upsilon|$ = 2, 4, 8, and 12 μm/s for blue, yellow, black, and green, respectively). The arrows indicate the start of Kip3p binding events. (**C**) Trap force as a function of stage position. After a transient phase, a plateau value (- - -) is reached. Data are from the same experiment as in (B); each trace is an average of several drag events. Similar results were found for eight other microtubules.

sites and the position of the energy barrier, which corresponds to a transition state (Fig. 3, schematic inset). Provided that the fluctuations in the force are small, as is the case (Fig. 2C and fig. S5), Eq. 1 relates the friction force $F = -F_{trap}$ to the stage velocity $\upsilon = -\upsilon_m$. In the limit of low forces, a Taylor expansion of Eq. 1 results in $\upsilon = [\delta^2 k_0/(k_B T)]F = F/\gamma$, corresponding to the linear force-velocity relation observed at low speeds.

A global fit of Eq. 1 to nine force-velocity curves obtained on nine different microtubules in different experiments encompassing a total of 2015 drag events (Fig. 3, graph inset, and table S1) gave a step distance $\delta = 7.8 \pm 0.3$ nm, an asymmetry parameter $\Delta = 0.33 \pm 0.01$ nm, and a stepping rate $k_0 = 90 \pm 15\ s^{-1}$. The spatial asymmetry, though small, can lead to large differences in translocation velocities, depending on the magnitude and direction of the force (Fig. 3).

To obtain direct evidence for stepwise movement along the lattice, we examined displacement traces recorded at intermediate velocities. We observed steps of roughly 8 nm in size (Fig. 4A). To objectively estimate step-sizes over the whole range of velocities, including the ones with poor signal-to-noise ratios, we performed a fluctuation analysis [Fig. 4B and fig. S6] (*24*). For $|\upsilon| \geq 4$ μm/s, we obtained an average step size $\delta = 7.9 \pm 0.3$ nm. At lower speeds, we expected to overestimate the step size because of the presence of backward steps (*9*) (Fig. 4B, inset, dashed line). However, we observed a decrease in step size, which suggested that several rate-limiting processes at low forces exist, as has been observed for kinesin-1 (*25*). Thus, the fluctuation analysis supports the direct observation of 8-nm steps during frictional slipping of the motor along the microtubule.

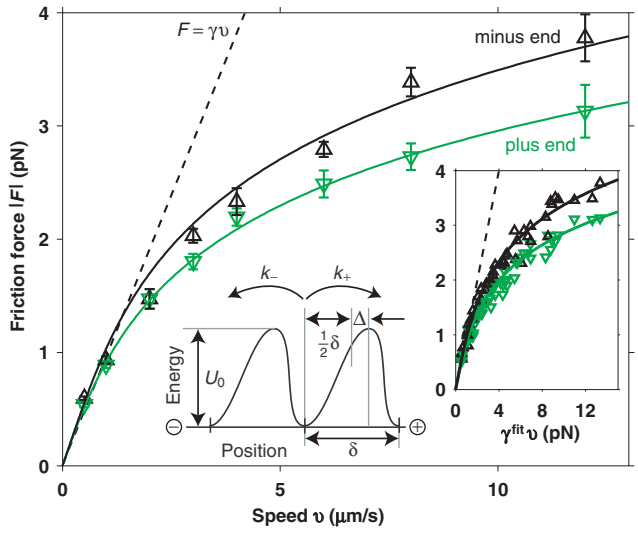

Fig. 3. Force-velocity relation. Absolute value of the friction force as a function of drag speed for the same Kip3p molecule and microtubule shown in Fig. 2, B and C. Drag direction toward the microtubule's plus end (▽) and minus end (△) are indicated. Theoretical force-velocity relations are based on (i) viscouslike friction $F = \gamma_{TIRF}\upsilon$ (- - -) and (ii) protein friction (fit with Eq. 1: directed toward the plus or minus end). (**Graph inset**) Master curve of nine sets of measurements from nine microtubules with a re-scaled abscissa: The stage speed is multiplied by the individual linear frictional drag coefficients for each microtubule-motor set. In this way, the linear force-velocity relation (- - -) has a slope of one. (**Schematic inset**) Asymmetric potential landscape defining the periodicity δ, the asymmetry parameter Δ, the potential well depth U_0, and the forward k_+ and backward k_- rates. The asymmetry in the schematic is exaggerated to illustrate the asymmetry parameter.

Considering both the velocity-dependence of the frictional force and the fluctuation analysis, we conclude that the motor's binding sites on the microtubule are spaced 8 nm apart and separated by a single activation barrier. By comparing the hydrodynamic drag coefficient of Kip3p in solution measured by fluorescence correlation spectroscopy, $20 \pm 2\ \mu m^2/s$ (fig. S3A), with the frictional drag coefficient on the microtubule and using a first-passage time analysis, we calculated the height of the energy barrier to be $U_0 = 13 \pm 2\ k_B T$ (*20*). Therefore, our measurements of protein friction allow us to estimate the asymmetric periodic interaction energy landscape between a molecular motor and its track, in a specific nucleotide state.

What is the molecular basis for the 8-nm steps? Our measured step size of ~8 nm suggests that during diffusion and the frictional interaction, Kip3p is stepping from one tubulin dimer [8.2 nm in length (*5*)] to the adjacent one and not following the periodicity imposed by the E-hooks. In support of this conclusion, we found that the diffusion coefficient and the interaction time were not

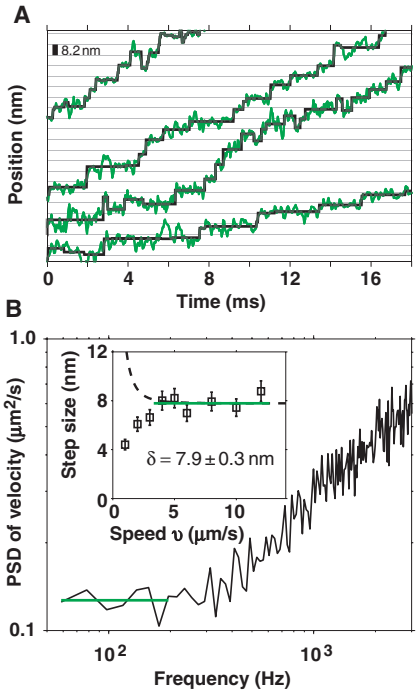

Fig. 4. Step determination methods. (**A**) Stepwise movement in exemplary regions (υ = 8 μm/s). The underlying grid has an 8.2-nm periodicity equal to the length of a tubulin dimer. Step detectors find steps consistent with ~8 nm. (**B**) Fluctuation analysis: Velocity power spectral density (PSD, drag velocity υ = 8 μm/s). The plateau $p = 2\upsilon\delta$ at low frequencies indicates that the microsphere moved in a stepwise manner (green horizontal line: average plateau value). (Inset) Step size based on the fluctuation analysis as a function of drag speed. The dashed line (- - -) shows the expected behavior for a Poisson stepper including backward steps. The green solid line indicates the mean step size value for $|\upsilon| \geq 4$ μm/s ($N = 6$).

greatly changed when the E-hook was removed by proteolysis (fig. S1). We therefore propose that Kip3p diffusion in the presence of ADP predominantly involves interactions with the canonical kinesin-tubulin–binding site. The long association time in ADP suggests that diffusion of Kip3p occurs via a hand-over-hand mechanism whereby the two motor domains bind to adjacent tubulin dimers along a protofilament, and that when one unbinds it can rebind either in front or behind the other motor domain.

In addition to providing information about the molecular mechanism of protein diffusion along microtubules, our measurement of protein friction provides mechanical insight into the speed and efficiency of Kip3p and other motors. In the conventional chemical view of molecular motors (*5*), mechanical motion is tightly coupled to transitions between different chemical states in the ATP hydrolysis cycle. The rates of the transitions, in turn, depend on the load. This picture can be turned around to produce a mechanical view of a molecular motor interacting with its track in which a force-generating element is opposed by a frictional element that dissipates energy and limits the speed (*26*). The friction arises because the breaking of bonds associated with chemical states slows the transitions between the mechanical states even in the presence of an external force. Kip3p is a very slow motor, with a maximum speed of 0.05 μm/s. Given that Kip3p can generate a force F_m larger than 1 pN (fig. S7), our measurement of the frictional drag coefficient in ADP of 0.75 μNs/m indicates that drag in the ADP state is not limiting the speed ($F_m/\gamma >> \upsilon_m$). Instead, the maximum speed of Kip3p is likely to be limited by the drag in strongly bound states, such as the nucleotide-free state with a frictional drag coefficient of ~20 μNs/m, as estimated from the diffusion coefficient. In contrast, measurements on kinesin-1 (*27*, *28*) indicate a frictional drag coefficient toward the microtubule plus end of ~10 μNs/m in ADP. Given that the maximum force is 7 pN (*29*) and that detachment in the ADP state is thought to be the rate-limiting step for kinesin-1 (*28*), we predict a maximum speed of 0.7 μm/s, similar to the maximum speed of kinesin-1.

Protein friction also gives insight into the efficiency of kinesin. The slope of the force-velocity curve can be interpreted as the friction coefficient of an active motor. For kinesin-1, this is ~8 μNs/m (the maximum force divided by the maximum speed). At maximum speed, such a friction element dissipates $\gamma\upsilon_m\delta \approx 50 \times 10^{-21}$ J per 8-nm step. Thus, about 50% of the energy from ATP hydrolysis (*5*) is dissipated as friction between the motor and its substrate. Internal conformational changes in the motor head associated with the ATP hydrolysis cycle lead to additional energy dissipation.

Protein friction is important in muscle (*30*) and should apply to other molecular motors, such as myosin V (*31*), DNA enzymes (*32*, *33*), and rotary engines (*34*, *35*). Diffusion of proteins along polymers and microtubules plays a central role in several biological processes, as discussed in the introduction. In the case of diffusion, no net energy is dissipated. In the case of actively driven proteins, energy should predominantly be dissipated through protein friction. Our single-molecule studies indicate that bond rupture dynamics underlie both diffusion and protein friction.

References and Notes

1. M. Urbakh, J. Klafter, D. Gourdon, J. Israelachvili, *Nature* **430**, 525 (2004).
2. E. Evans, *Annu. Rev. Biophys. Biomol. Struct.* **30**, 105 (2001).
3. J. Helenius, C. P. Heisenberg, H. E. Gaub, D. J. Müller, *J. Cell Sci.* **121**, 1785 (2008).
4. H. Suda, *Langmuir* **17**, 6045 (2001).
5. J. Howard, *Motor Proteins and the Cytoskeleton* (Sinauer Associates, Sunderland, MA, 2001).
6. K. Tawada, K. Sekimoto, *J. Theor. Biol.* **150**, 193 (1991).
7. A. Parmeggiani, F. Jülicher, A. Ajdari, J. Prost, *Phys. Rev. E Stat. Phys. Plasmas Fluids Relat. Interdiscip. Topics* **60**, 2127 (1999).
8. M. E. Fisher, A. B. Kolomeisky, *Proc. Natl. Acad. Sci. U.S.A.* **96**, 6597 (1999).
9. N. Thomas, Y. Imafuku, K. Tawada, *Proc. R. Soc. Lond. B. Biol. Sci.* **268**, 2113 (2001).
10. J. Helenius, G. Brouhard, Y. Kalaidzidis, S. Diez, J. Howard, *Nature* **441**, 115 (2006).
11. G. J. Brouhard *et al.*, *Cell* **132**, 79 (2008).
12. S. Westermann *et al.*, *Nature* **440**, 565 (2006).
13. A. F. Powers *et al.*, *Cell* **136**, 865 (2009).
14. L. C. Kapitein *et al.*, *Curr. Biol.* **18**, 1713 (2008).
15. K. Furuta, Y. Y. Toyoshima, *Curr. Biol.* **18**, 152 (2008).
16. Y. Okada, N. Hirokawa, *Proc. Natl. Acad. Sci. U.S.A.* **97**, 640 (2000).
17. V. Varga *et al.*, *Nat. Cell Biol.* **8**, 957 (2006).
18. M. L. Gupta, P. Carvalho, D. M. Roof, D. Pellman, *Nat. Cell Biol.* **8**, 913 (2006).
19. G. Goshima, R. Wollman, N. Stuurman, J. M. Scholey, R. D. Vale, *Curr. Biol.* **15**, 1979 (2005).
20. Materials and methods are available as supporting material on *Science* Online.
21. E. Schäffer, S. F. Nørrelykke, J. Howard, *Langmuir* **23**, 3654 (2007).
22. V. Bormuth *et al.*, *Opt. Express* **16**, 13831 (2008).
23. S. F. Tolić-Nørrelykke *et al.*, *Rev. Sci. Instrum.* **77**, 103101 (2006).
24. G. Charvin, D. Bensimon, V. Croquette, *Single Mol.* **3**, 43 (2002).
25. K. Svoboda, P. P. Mitra, S. M. Block, *Proc. Natl. Acad. Sci. U.S.A.* **91**, 11782 (1994).
26. J. Howard, *Annu. Rev. Biophys.* **38**, 217 (2009).
27. S. Uemura, S. Ishiwata, *Nat. Struct. Biol.* **10**, 308 (2003).
28. A. Yildiz, M. Tomishige, A. Gennerich, R. D. Vale, *Cell* **134**, 1030 (2008).
29. N. J. Carter, R. A. Cross, *Nature* **435**, 308 (2005).
30. B. Brenner, M. Schoenberg, J. M. Chalovich, L. E. Greene, E. Eisenberg, *Proc. Natl. Acad. Sci. U.S.A.* **79**, 7288 (1982).
31. J. C. M. Gebhardt, A. E.-M. Clemen, J. Jaud, M. Rief, *Proc. Natl. Acad. Sci. U.S.A.* **103**, 8680 (2006).
32. E. A. Galburt *et al.*, *Nature* **446**, 820 (2007).
33. D. A. Koster, V. Croquette, C. Dekker, S. Shuman, N. H. Dekker, *Nature* **434**, 671 (2005).
34. H. C. Berg, *Annu. Rev. Biochem.* **72**, 19 (2003).
35. K. Kinosita, K. Adachi, H. Itoh, *Annu. Rev. Biophys. Biomol. Struct.* **33**, 245 (2004).

36. We thank J. Mütze and P. Schwille for the fluorescence correlation spectroscopy measurements; R. Seidel and S. Grill for helpful discussions; the latter two, G. Brouhard, M. Zanic, C. Gell, B. Nitzsche, S. Nørrelykke, H. Flyvbjerg, M. Fisher, and S. Diez for comments on the manuscript; F. Zörgiebel for help in the assay development; H. Flyvbjerg additionally for the error estimates of correlated data; Y. Kalaidzidis and Transinsight GmbH for the image analysis software; and Gausepohl Fleisch GmbH for the pig brains. The work was supported by the Deutsche Forschungsgemeinschaft (E. Noether Program), the Max Planck Society, and the Technische Universität Dresden. V.B. had a fellowship from the Boehringer Ingelheim Fonds. Author contributions were as follows: V.B., J.H., and E.S. designed research; V.B. (optical tweezers) and V.V. (protein purification, TIRF) performed research; V.B., V.V., and E.S. analyzed data; J.H. provided advice; and V.B., J.H., and E.S. wrote the paper.

Supporting Online Material

www.sciencemag.org/cgi/content/full/325/5942/870/DC1
Materials and Methods
SOM Text
Figs. S1 to S7
Table S1
References

13 April 2009; accepted 8 July 2009
10.1126/science.1174923